Journal of Alloys and Compounds 564 (2013) 117–124

Contents lists available at SciVerse ScienceDirect

Journal of Alloys and Compounds

journal homepage: www.elsevier.com/locate/jalcom

Structural, electronic properties, and chemical bonding in quaternary layered titanium pnictide-oxides $Na_2Ti_2Pn_2O$ and $BaTi_2Pn_2O$ (*Pn* = As, Sb) from FLAPW–GGA calculations

D.V. Suetin, A.L. Ivanovskii *

Institute of Solid State Chemistry, Ural Branch of the Russian Academy of Sciences, GSP-145, Ekaterinburg 620990, Russia

ARTICLE INFO

Article history:
Received 14 January 2013
Received in revised form 22 February 2013
Accepted 27 February 2013
Available online 7 March 2013

Keywords:
Layered $Na_2Ti_2Pn_2O$
$BaTi_2Pn_2O$
Electronic properties
chemical bonding
Fermi surfaces
First-principles calculations

ABSTRACT

By means of the first-principles FLAPW–GGA calculations, we have investigated the main trends in structural, electronic properties, and chemical bonding for a series of quaternary titanium pnictide-oxides: $Na_2Ti_2As_2O$, $Na_2Ti_2Sb_2O$, $BaTi_2As_2O$, and $BaTi_2Sb_2O$, which attracted now much attention as parent phases for a novel group of layered Fe-free superconducting materials. Our results cover the optimized lattice parameters and atomic positions, electronic bands, Fermi surface topology, total and partial density of electronic states. Besides, Bader analysis and the charge density maps are used to discuss the chemical bonding for the examined materials. We find that the atomic substitutions lead to anisotropic deformation of the crystal structure; this effect is related to strong anisotropy of inter-atomic bonds, which are of a mixed (covalent-ionic-metallic) type – in blocks $[Ti_2Pn_2O]$, whereas the bonding between blocks $[Ti_2Pn_2O]$ and atomic sheets of Na, Ba ions is of an ionic type. The actual effective atomic charges differ from the formal ionic charges due to covalency in blocks $[Ti_2Pn_2O]$. The near-Fermi electronic bands, which are responsible for metallic-like behavior of these materials and will be involved in the formation of superconducting state, arise mainly from the Ti $3d_{xy}$, d_{x2-y2}, and d_{z2} states of the blocks $[Ti_2Pn_2O]$, which define also the anisotropic character of conduction happening mainly in these blocks. The differences in the topology of the multi-sheet Fermi surfaces of these materials are discussed.

1. Introduction

The discovery of superconductivity in layered Fe–*Pn* [1] and Fe–*Ch* [2] materials (where *Pn* and *Ch* are pnictogens and chalcogens, respectively), for which superconductivity emerges in $[Fe_2Pn_2]$ or $[Fe_2Ch_2]$ blocks, has stimulated intense efforts in search for new layered superconductors (SCs) and comprehensive investigations of their properties, see reviews [3–10]. As a result, a number of new layered compounds with quite unusual structures and compositions were found recently as possible SCs. Among them there are multi-component phases: so-called 32225 (such as $Sr_3Sc_2Fe_2As_2O_5$ [11]) and 42226 compounds ($A_4M_2Fe_2Pn_2O_6$, where *M* and *A* are transition- and alkaline-earth metals, respectively [12–19]) and a homologous series $(Fe_2As_2)(Ca_{n+1}(Sc,Ti)_nO_y)$, where $n = 3$, 4, 5 and $y \sim 3n - 1$ [20]. These phases also include superconducting blocks $[Fe_2Pn_2]$, which are separated by thick perovskite-like blocks: $[A_3M_2O_5]$, $[A_4M_2O_6]$ or $[Ca_{n+1}(Sc,Ti)_nO_y]$. As examples of other interesting Fe-containing SCs, it is worth noting $Ca_{10}(Pt_3As_8)(Fe_2As_2)_5$, $Ca_{10}(Pt_4As_8)(Fe_2As_2)_5$ (so-called 10-3-8 and 10-4-8 phases) [21,22], and $Sr_2CuFe_2As_2O_2$, which unite two types of main building blocks of two broad families of high-T_C superconductors: cuprates (blocks $[CuO_2]$) and iron-pnictides (blocks $[Fe_2As_2]$) [23–25].

Besides superconductivity, the aforementioned materials exhibit a huge variety of exciting physical properties such as charge or spin density waves (CDW or SDW), different types of magnetic ordering, coexistence of SC and CDW/SDW phases, as well as coexistence of magnetism and superconductivity etc., reviews [3–10,19].

Another line in the development of the new layered SCs is the search for Fe-free materials. Very recently, the quaternary layered titanium pnictide-oxides such as $BaTi_2Sb_2O$ and $Na_2Ti_2Sb_2O$ (which are sometimes represented by the general formula ATi_2Pn_2O, where $A = Ba^{2+}$ or $2Na^{1+}$) attracted much attention [26,27]. Indeed, a low-T_C superconducting transition at 1.2 K was found for $BaTi_2Sb_2O$ [26] and for hole-doped $Ba_{1-x}Na_xTi_2Sb_2O$ ($0.0 \leqslant x \leqslant 0.33$) and an increase in T_C to 5.5 K (for $x \sim 0.33$) was established [27]. The authors [26,27] pointed out also that (i) in $BaTi_2Sb_2O$ the orbital configurations of trivalent cations $Ti^{3+}(d^1)$ in mixed anionic coordination $\{O_2Sb_2\}$ resemble the same for $Cu^{2+}(d^9)$ in high-T_C cuprates; and (ii) CDW/SDW instability in $BaTi_2Sb_2O$ emerges at $T_S \sim 50$ K, which is much lower than for $BaTi_2As_2O$ ($T_S \sim 200$ K). Note that a drastic reduction in T_S was also

* Corresponding author. Tel.: +7 3433745331; fax: +7 343 3744495.
E-mail address: ivanovskii@ihim.uran.ru (A.L. Ivanovskii).

0925-8388/$ - see front matter © 2013 Elsevier B.V. All rights reserved.
http://dx.doi.org/10.1016/j.jallcom.2013.02.155

found for isoelectronic analogues of $BaTi_2Pn_2O$, i.e. as going from $Na_2Ti_2As_2O$ ($T_S \sim 330$ K) to $Na_2Ti_2Sb_2O$ ($T_S \sim 120$ K) [28–34]. Taking into consideration that $BaTi_2As_2O$ is non-superconducting [30], these results give a clear hint that at least two alternative ways may lead to superconductivity of ATi_2Pn_2O owing to: (i) hole doping (as in the case of $Ba_{1-x}Na_xTi_2Sb_2O$) or (ii) isovalent atomic substitutions (without carriers doping) – as in the case of $BaTi_2As_2O \rightarrow BaTi_2Sb_2O$, where the replacement of As^{3-} by Sb^{3-} anions with larger radii leads to suppression of CDW/SDW instability and to emergence of superconducting state [26]. Further confirmation of the latter trend follows from the newest data [35], where an enhanced $T_C \sim 4.6$ K was established for $BaTi_2Bi_2O$ ($R(As^{3-}) < R(Sb^{3-}) < R(Bi^{3-})$). The correlation effects in $Na_2Ti_2Sb_2O$ estimated experimentally are weak [36].

Theoretically the first data about the electronic structure of $Na_2Ti_2Sb_2O$ were obtained, as far as we know, within the extended Hückel tight-binding method [29], and further the *ab initio* full potential linearized augmented plane wave (FLAPW) method [37] and the plane wave basis method within the PW91-type generalized gradient approximation (GGA) [38] were applied for this material. Besides, very recently, two similar works [39,40] were performed to clarify theoretically some peculiarities of the electronic band structure, phonon dispersions, and electron–phonon coupling for $BaTi_2Sb_2O$ [40] and hole-doped $Ba_{1-x}Na_xTi_2Sb_2O$ [39].

In order to get a systematic insight into the basic structural, electronic properties and the peculiarities of chemical bonding in quaternary layered titanium pnictide-oxides, in this work we carried out a first-principles study of four phases, namely $Na_2Ti_2As_2O$, $Na_2Ti_2Sb_2O$, $BaTi_2As_2O$, and $BaTi_2Sb_2O$. This series allows us to compare the aforementioned properties depending on (i) the type of the crystal structure ($Na_2Ti_2As_2O$ and $Na_2Ti_2Sb_2O$ versus $BaTi_2As_2O$ and $BaTi_2Sb_2O$); (ii) type of the metal *A* (Na versus Ba), and (iii) the type of pnictogen (As versus Sb). Our results cover the optimized lattice parameters and atomic positions, electronic bands, Fermi surface topology, as well as total and partial density of electronic states. Besides, Bader analysis and the charge density maps are used in discussing the chemical bonding for the examined materials.

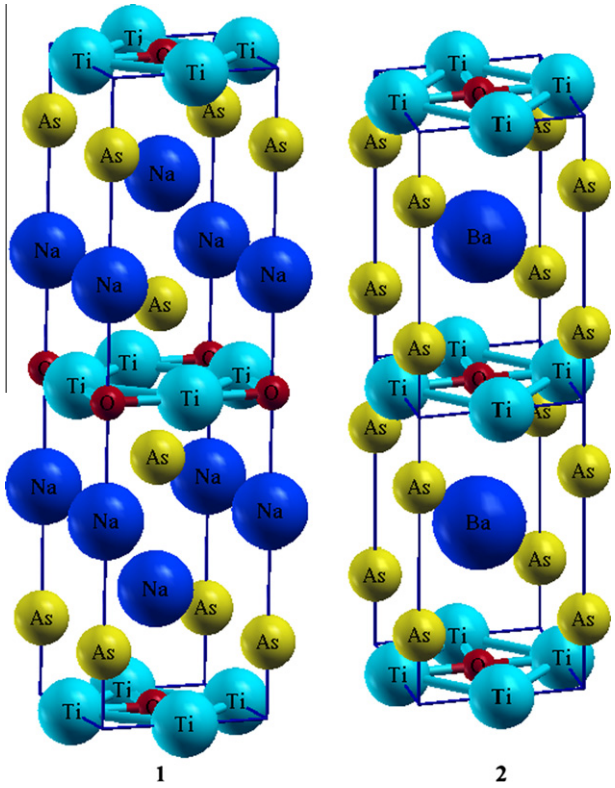

Fig. 1. Crystal structures of (1) $Na_2Ti_2As_2O$ ($Na_2Ti_2Sb_2O$) and (2) $BaTi_2As_2O$ ($BaTi_2Sb_2O$).

Table 1
Optimized atomic positions for $Na_2Ti_2As_2O$, $Na_2Ti_2Sb_2O$, $BaTi_2As_2O$, and $BaTi_2Sb_2O$.

Atomic positions	*x*	*y*	*z*[a]
$Na_2Ti_2As_2O$			
Na (4*e*)	0	0	0.3185
Ti (4*c*)	0	0.5	0
As (4*e*)	0	0	0.1180
O (2*b*)	0	0	0.5
$Na_2Ti_2Sb_2O$			
Na (4*e*)	0	0	0.3179 (0.3188[b]; 0.3179[c])
Ti (4*c*)	0	0.5	0
Sb (4*e*)	0	0	0.1211 (0.1218[b]; 0.1212[c])
O (2*b*)	0	0	0.5
$BaTi_2As_2O$			
Ba (1*d*)	0.5	0.5	0.5
Ti (2*f*)	0.5	0	0
As (2*g*)	0	0	0.7573 (0.7560[d])
O (1*c*)	0.5	0.5	0
$BaTi_2Sb_2O$			
Ba (1*d*)	0.5	0.5	0.5
Ti (2*f*)	0.5	0	0
Sb (2*g*)	0	0	0.7533 (0.7514[e]; 0.7486[f]; 0.7507[g])
O (1*c*)	0.5	0.5	0

[a] Available results are given in parentheses.
[b] Ref. [30], experiment, powder neutron diffraction at 105 K.
[c] Ref. [45], experiment, XRD.
[d] Ref. [34], experiment, XRD.
[e] Ref. [26], experiment, synchrotron XRD.
[f] Ref. [27], experiment, XRD.
[g] Ref. [40], calculated, Quantum-ESPRESSO package.

2. Models and computational aspects

The considered phases $Na_2Ti_2As_2O$, $Na_2Ti_2Sb_2O$, $BaTi_2As_2O$, and $BaTi_2Sb_2O$ have a tetragonal structure. Among them, $Na_2Ti_2As_2O$ and $Na_2Ti_2Sb_2O$ have the space group *I*4/*mmm* and can be described as a stacking of blocks $[Ti_2Pn_2O]^{2-}$ and double sheets of Na^{1+} ions, Fig. 1. In turn, each block $[Ti_2Pn_2O]$ consists of a Ti_2O square plane (with anti-CuO_2 configuration) placed between two *Pn* atomic layers, where *Pn* atoms are arranged symmetrically above and below the center of Ti squares, see [30]. The phases

Table 2
Optimized lattice constants (*a* and *c*, in Å) and cell volumes (V, in nm^3) for $Na_2Ti_2As_2O$, $Na_2Ti_2Sb_2O$, $BaTi_2As_2O$, and $BaTi_2Sb_2O$.

System	*a*[a]	*c*[a]	*V*[a]
$Na_2Ti_2As_2O$	4.0716 (4.070[c]; 4.079[d]; 4.060[h])	15.3941 (15.288[c]; 15.26[d]; 15.389[h])	0.12760 (0.12662[c])
$Na_2Ti_2Sb_2O$	4.1508 (4.1494[b]; 4.144[c]; 4.153[d]; 4.137[h])	16.8149 (16.4671[b]; 16.561[c]; 16.57[d]; 16.643[h])	0.14485 (0.14220[c])
$BaTi_2As_2O$	4.0571 (4.0456[e])	7.2634 (7.2723[e])	0.11956
$BaTi_2Sb_2O$	4.1155 (4.1104[f]; 4.1196[g])	8.1700 (8.0864[f]; 8.0951[g])	0.13838 (0.13738[g])

[a] Available results are given in parentheses.
[b] Ref. [30], experiment, powder neutron diffraction at 105 K.
[c] Ref. [45], experiment, XRD.
[d] Ref. [33], experiment, XRD.
[e] Ref. [34], experiment, XRD.
[f] Ref. [26], experiment, synchrotron XRD.
[g] Ref. [27], experiment, XRD.
[h] Ref. [38], calculated, PW-basis method within the PW91-type generalized gradient approximation.

$BaTi_2As_2O$ and $BaTi_2Sb_2O$ have the space group $P4/mmm$ with the same blocks [Ti_2Pn_2O], which alternate with single sheets of Ba^{2+} ions, Fig. 1. The crystal structures of all the considered phases ATi_2Pn_2O are defined by the lattice parameters a and c and the internal parameters z_{Na} and z_{Pn} for $Na_2Ti_2As_2O$ and $Na_2Ti_2Sb_2O$ and z_{Pn} for $BaTi_2As_2O$ and $BaTi_2Sb_2O$.

The calculations were performed by means of the full-potential linearized augmented plane wave method with mixed basis APW + lo (FLAPW) implemented in the WIEN2k suite of programs [41]. The generalized gradient approximation (GGA) to exchange-correlation potential in the well-known PBE form [42] was used. The basis set inside each muffin tin (MT) sphere was split into core and valence subsets. The core states were treated within the spherical part of the potential only and were assumed to have a spherically symmetric charge density in MT spheres. The valence part was treated with the potential expanded into spherical harmonics to $l = 4$. The valence wave functions inside the spheres were expanded to $l = 12$. We used corresponding atomic radii: 2.00 a.u. for Na, 2.10 for Ba, 1.90 a.u. for Ti, 2.10 a.u. for As and Sb, and 1.70 a.u. for O atoms. The plane-wave expansion was taken to $R_{MT} \times K_{MAX}$ equal to 7, and the k sampling with $10 \times 10 \times 10$ k-points for $Na_2Ti_2Pn_2O$ and $12 \times 12 \times 6$ k-points for $BaTi_2Pn_2O$ in the Brillouin zone was used. The self-consistent calculations were considered to be converged when the difference in the total energy of the crystal did not exceed 0.1 mRy as calculated at consecutive steps, see also Supporting information.

The hybridization effects were analyzed using the densities of states (DOSs), which were obtained by the modified tetrahedron method [43], and some peculiarities of the chemical bonding picture were visualized by means of electronic density maps. To describe ionic bonding, a Bader's analysis [44] was carried out.

3. Results and discussion

3.1. Structural properties

As the first step, the equilibrium lattice constants (a and c) for ATi_2Pn_2O phases were calculated with full structural optimization including internal parameters z_{Na} and z_{Pn}. The results obtained are listed in Tables 1 and 2 and are in reasonable agreement with the available experimental and theoretical data. We see that in the sequences $Na_2Ti_2As_2O \rightarrow Na_2Ti_2Sb_2O$ and $BaTi_2As_2O \rightarrow BaTi_2Sb_2O$ (i.e. at substitution As → Sb in the isostructural crystals), the lattice parameters a and c increase by ~1.9% and 9.2% ($Na_2Ti_2Pn_2O$) and by 1.4% and 11.2% (for $BaTi_2Pn_2O$). This is easy to explain taking into account the atomic radii of pnictogens: R(As) = 1.14 Å < R(Sb) = 1.33 Å [46]. On the other hand, the parameter c (i.e. inter-blocks distance) grows much more appreciably (by about 9–11%) than the parameter a (by about 1.4–1.9%); thus, an *anisotropic* deformation of crystals takes place at isovalent substitutions. This effect was pointed out for a number of layered phases (reviews [3–10,19]), and it is related to strong *anisotropy of interatomic bonds*; in our case – strong bonds inside blocks [Ti_2Pn_2O] versus relatively weak ionic coupling between adjacent blocks [Ti_2Pn_2O] and the sheets of Na^{1+} or Ba^{2+} ions, see below.

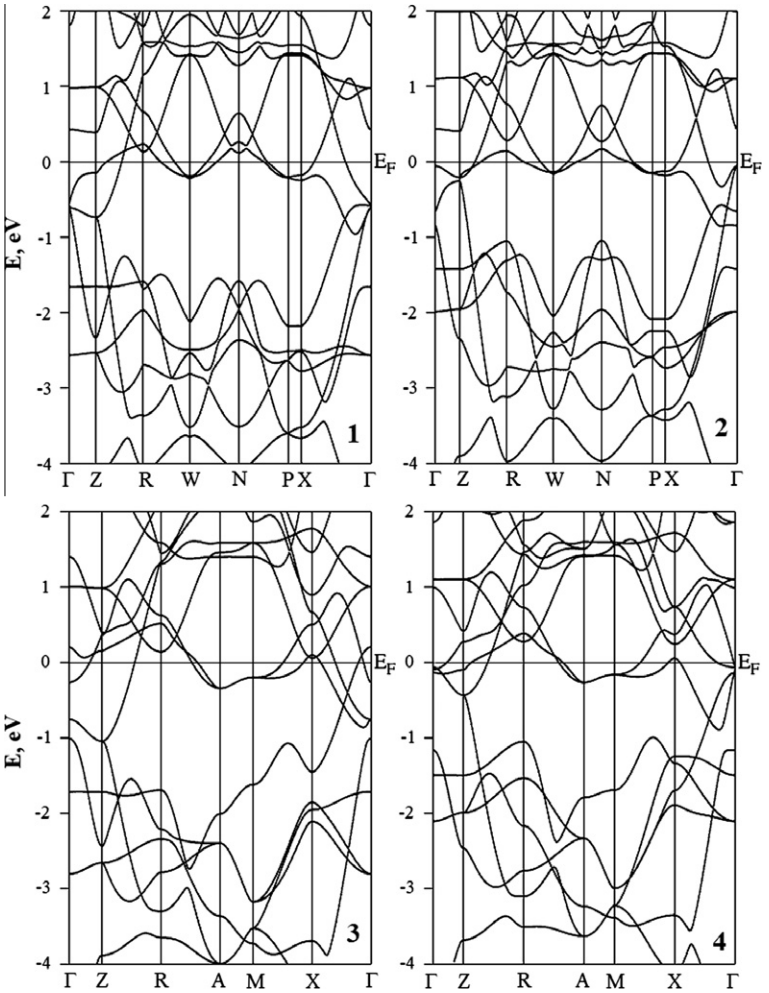

Fig. 2. Calculated near-Fermi electronic bands for $Na_2Ti_2As_2O$ (1), $Na_2Ti_2Sb_2O$ (2), $BaTi_2As_2O$ (3), and $BaTi_2Sb_2O$ (4).

In the sequences $Na_2Ti_2As_2O \rightarrow BaTi_2As_2O$ and $Na_2Ti_2Sb_2O \rightarrow BaTi_2Sb_2O$ (i.e. at replacement of a double sheet of Na^{1+} ions by a single sheet of Ba^{2+} ions), the main effect is a considerable reduction of the parameter c – by about 53% for ATi_2As_2O and by about 51% for ATi_2Sb_2O. Simultaneously, a weak reduction of the parameter a is found, see Table 2.

3.2. Electronic properties and Fermi surfaces

The near-Fermi electronic bands and total and partial densities of states (DOSs) of the examined phases ATi_2Pn_2O are depicted in Figs. 2 and 3. Generally, the valence spectra of ATi_2Pn_2O can be divided into several parts: (i) lowest quasi-core bands, which are formed predominantly by O 2s states and *Pn* s states, are centered about −20 eV and −11 eV (for arsenides) or −10 eV (for antimonides)

Table 3
Calculated bandwidths (in eV) for separate occupied bands and the band gaps (BGs) for $Na_2Ti_2As_2O$, $Na_2Ti_2Sb_2O$, $BaTi_2As_2O$, and $BaTi_2Sb_2O$ from FLAPW–GGA calculations.

System	O 2*s*	BG	Ba 5*p*	BG	*Pn* s
$Na_2Ti_2As_2O$	1.21	–	–	7.99	1.40
$Na_2Ti_2Sb_2O$	1.06	–	–	8.89	1.67
$BaTi_2As_2O$	1.20	5.05	1.10	1.66	1.54
$BaTi_2Sb_2O$	1.08	4.78	0.96	3.09	1.74
	BG	O 2*p*[a]	BG[a]	Valence band (up to E_F)	
$Na_2Ti_2As_2O$	2.26	2.71	0.08	7.66	
$Na_2Ti_2Sb_2O$	1.26	–	–	7.21	
$BaTi_2As_2O$	2.29	–	–	7.62	
$BaTi_2Sb_2O$	1.19	–	–	7.28	

[a] For $Na_2Ti_2Sb_2O$, $BaTi_2As_2O$, and $BaTi_2Sb_2O$, the O 2*p*-like bands and the next near-Fermi bands are merged.

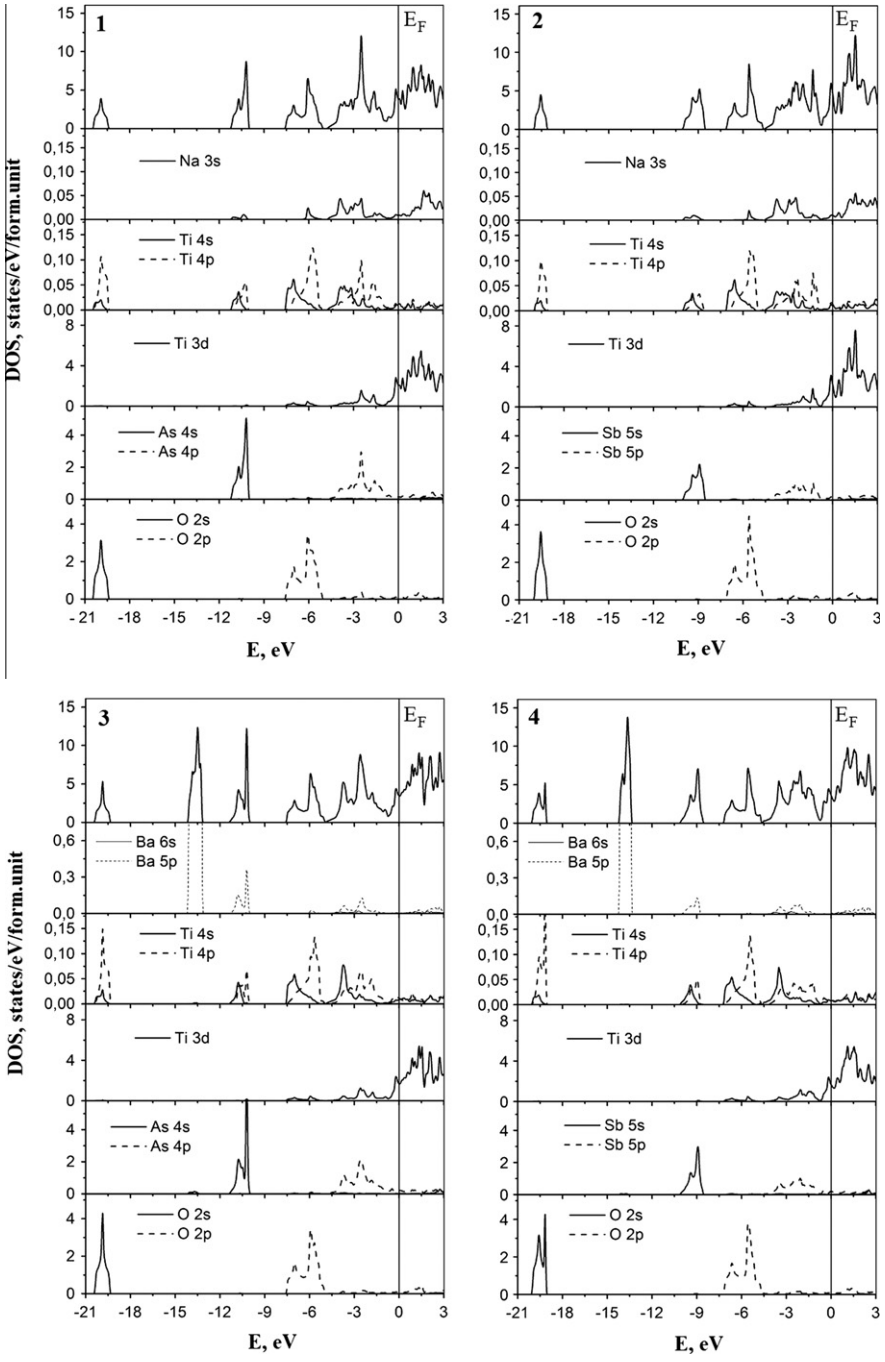

Fig. 3. Total and partial densities of states for $Na_2Ti_2As_2O$ (1), $Na_2Ti_2Sb_2O$ (2), $BaTi_2As_2O$ (3), and $BaTi_2Sb_2O$ (4).

Table 4
Calculated total and partial densities of states at the Fermi level $N(E_F)$ (in states/eV/form.unit), electronic heat capacity γ (in mJ K^{-2} mole^{-1}), and molar Pauli paramagnetic susceptibility (in 10^{-4} emu/mole) for $Na_2Ti_2As_2O$, $Na_2Ti_2Sb_2O$, $BaTi_2As_2O$, and $BaTi_2Sb_2O$ phases.

System	Total	Ti 3*d*	Na, Ba *s, p*	*Pn p*	O 2*p*	γ	χ
$Na_2Ti_2As_2O$	3.834 (3.84[b])	2.060	0.008	0.148	0.049	9.04 (9.05[b])	1.24
$Na_2Ti_2Sb_2O$	4.677 (4.40[b])	2.253	0.010	0.210	0.077	11.03 (10.37[b])	1.51
$BaTi_2As_2O$	3.467	1.695	0.008	0.215	0.061	8.18	1.12
$BaTi_2Sb_2O$	3.599 (4.26[c])	1.672	0.012	0.189	0.069	8.49 (10.0[c])	1.16 (1.37[c])

[a] Available theoretical results are given in parentheses.
[b] Ref. [38], PW-basis method within the PW91-type generalized gradient approximation.
[c] Ref. [39], WIEN2 k code.

Table 5
Orbital-resolved densities of states at the Fermi level of Ti 3*d* and (*Pn*, O) *p* states for $Na_2Ti_2As_2O$, $Na_2Ti_2Sb_2O$, $BaTi_2As_2O$, and $BaTi_2Sb_2O$ phases.

System	Ti $3d_{x2-y2}$	Ti $3d_{xy}$	Ti $3d_{z2}$	Ti $3d_{xz}$	Ti $3d_{yz}$
$Na_2Ti_2As_2O$	0.337	0.622	1.069	0.024	0.008
$Na_2Ti_2Sb_2O$	0.449	0.722	1.070	0.004	0.008
$BaTi_2As_2O$	0.302	0.622	0.692	0.034	0.045
$BaTi_2Sb_2O$	0.348	0.600	0.688	0.029	0.007
	Pn p_z	*Pn* p_{x+y}	O $2p_z$	O $2p_{x+y}$	
$Na_2Ti_2As_2O$	0.092	0.056	0.002	0.047	
$Na_2Ti_2Sb_2O$	0.058	0.152	0.003	0.074	
$BaTi_2As_2O$	0.138	0.077	0.006	0.055	
$BaTi_2Sb_2O$	0.071	0.118	0.006	0.063	

below the Fermi level (E_F), respectively; (ii) a group of electronic bands of hybridized (O 2*p*–Ti *s,p,d*) type placed around −6 eV, which are responsible for covalent O–Ti bonds; (iii) a group of hybridized bands composed of overlapped *Pn p* and Ti 3*d* orbitals (which form directional Ti–*Pn* bonds) centered at −3 eV (arsenides) or at −2 eV (antimonides); and (iv) a group of near-Fermi bands, which are composed mainly of Ti 3*d* states. The obvious difference between $Na_2Ti_2Pn_2O$ and $BaTi_2Pn_2O$ phases is the composition of the quasi-core states in the energy interval from −21 eV to −8 eV, where for the Na-containing phases only O 2*s* and *Pn s* states are located, while for the Ba- containing phases, additional Ba 5*p* states appear between these bands. The calculated bandwidths of these bands for all of the examined phases ATi_2Pn_2O are given in Table 3.

Since electrons near the Fermi level are involved in the formation of the superconducting state, it is important to understand their nature. The total and atomic decomposed partial DOSs at the Fermi level, $N(E_F)$, are shown in Table 4. It is seen that for all the examined phases ATi_2Pn_2O the main contribution to $N(E_F)$ comes from the Ti 3*d* states, which are responsible for the metallic-like properties of these materials. In turn, the values of $N^{tot}(E_F)$ increase in the sequences $Na_2Ti_2As_2O \rightarrow Na_2Ti_2Sb_2O$ and $BaTi_2As_2O \rightarrow BaTi_2Sb_2O$ first of all owing to the growth of contributions from the Ti 3*d* states at E_F, Table 4. In other words: (i) ATi_2Sb_2O phases have higher values of $N(E_F)$ than isostructural arsenides; (ii) transition from $BaTi_2Pn_2O$ to $Na_2Ti_2Pn_2O$ phases leads to an increase in $N(E_F)$. Thus, we can speculate that the appearance of superconductivity in the $Ba_{1-x}Na_xTi_2Sb_2O$ system may be associated (besides other factors, see [39,40]) with the growth of the density of states near the Fermi level owing to partial Na–Ba substitution.

The obtained data were used to evaluate the Sommerfeld constants (γ) and the Pauli paramagnetic susceptibility (χ), which are listed in Table 4. In turn, using the calculated γ^{theor}, we can estimate the average electron–phonon coupling constant λ within the simplified approximation [47] $\gamma^{exp} = \gamma^{theor}(1 + \lambda)$. For $BaTi_2Sb_2O$, $\gamma^{exp} = 13.5$ mJ K^{-2} mole^{-1} [26]; thus, the calculated $\lambda \sim 0.59$, i.e. this material is close to the weak coupling limit.

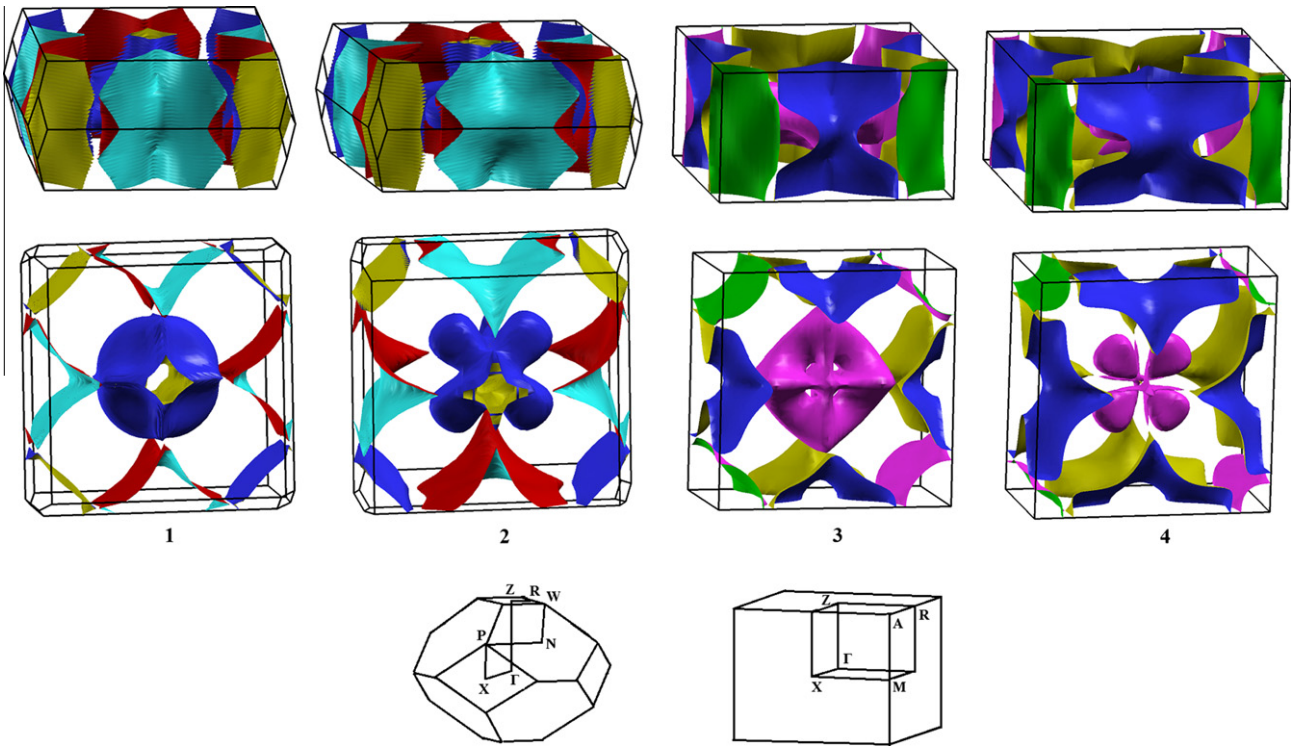

Fig. 4. Fermi surfaces for $Na_2Ti_2As_2O$ (1), $Na_2Ti_2Sb_2O$ (2), $BaTi_2As_2O$ (3), and $BaTi_2Sb_2O$ (4). *Bottom panel*: the corresponding Brillouin zones.

Coming back to the electronic properties of ATi_2Pn_2O, in Table 5 we summarize the orbital-resolved DOSs at the Fermi level for Ti 3*d* and (*Pn*, O) *p* states. As can be seen, the d_{xz} and d_{yz} orbitals from the Ti atoms give very little contributions to $N(E_F)$. These orbitals are directed towards *Pn* atoms forming covalent Ti 3*d*–*Pn p* bonds and are therefore shifted above and below of the Fermi level. On the contrary, the three other orbitals: d_{xy} (which form metal–metal bonds between the neighboring Ti atoms), d_{x2-y2} (directed to O^{2-} ions), and d_{z2} (directed along the *c* axis) give the main contributions to $N(E_F)$. Thus, these three orbitals participating in the formation of the quasi-flat near-Fermi bands define the main features of the Fermi surfaces (FSs), Fig. 4.

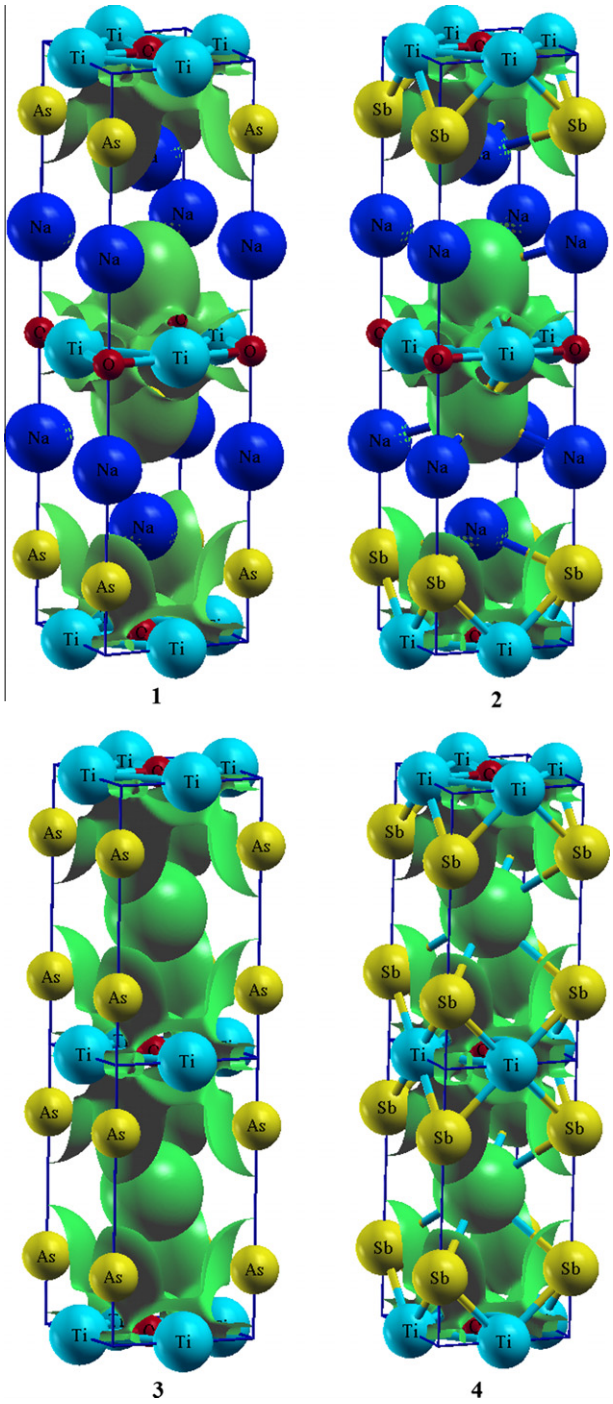

Fig. 5. Isosurfaces of electronic density (ρ = 0.2 e/Å^3) for $Na_2Ti_2As_2O$ (1), $Na_2Ti_2Sb_2O$ (2), $BaTi_2As_2O$ (3), and $BaTi_2Sb_2O$ (4).

We see that for all the examined phases ATi_2Pn_2O, their multi-sheet FSs are quite complicated and contain a set of hole-type and electron-type pockets. Generally, the FSs for $Na_2Ti_2As_2O$ and $Na_2Ti_2Sb_2O$ can be characterized as 2D-like. So, the FS for $Na_2Ti_2As_2O$ includes hole-type sheets in the form of disconnected deformed cylinders (which are centered at the *N* points of the BZ and are extended along the k_z direction) together with electron-like sheets. Among them the sheets placed in the corners of the BZ are also tube-like, whereas the next sheet with a complicated convex topology and with a square-shaped section is centered at the Γ point. The main difference in the FS for $Na_2Ti_2Sb_2O$ is due to further deformation of the electron-like sheet centered at the Γ point, which adopts a rosette-like form with "petals" directed along Γ–*X*, Fig. 4.

Unlike the discussed phases $Na_2Ti_2Pn_2O$, the multi-sheet FSs for $BaTi_2Pn_2O$ include also closed hole-like pockets centered at Γ, Fig. 4, together with 2D-like hole- and electron-type sheets in the form of deformed cylinders (on the lateral sides and in the corners of the BZ, respectively), which are extended along the k_z direction.

3.3. Inter-atomic bonding

According to our calculations, the common picture of inter-atomic interactions for all ATi_2Pn_2O phases can be described as a high-anisotropic mixture of metallic, covalent, and ionic contributions, where the *metallic-like* bonding is due mainly to the interaction of Ti $3d_{xy}$ orbitals of neighboring Ti atoms inside blocks $[Ti_2Pn_2O]$. In turn, *covalent* bonds also arise inside blocks $[Ti_2Pn_2O]$ as a result of hybridization of Ti–*Pn* and Ti–O valence states, see above. The in-block covalent bonding for ATi_2Pn_2O, as well as the *ionic* bonding between blocks $[Ti_2Pn_2O]$ and atomic *A* sheets are well visible from the electron density iso-surfaces depicted in Fig. 5.

In more details, the aforementioned bonds are illustrated using the charge density maps in (1 1 0) planes for $Na_2Ti_2As_2O$ and $Na_2Ti_2Sb_2O$, Fig. 6. Herein we can see that in the sequence $Na_2Ti_2As_2O \rightarrow Na_2Ti_2Sb_2O$, all of the bonds (Ti–*Pn*, Ti–O, and Ti–Ti) will be simultaneously weakened. It is quite expected effect (which occurs also for a pair $BaTi_2As_2O$ versus $BaTi_2Sb_2O$) – because of growth of lattice parameters at substitution As → Sb, see above.

As to ionic bonding, the widely used simplified ionic model assuming the oxidation numbers of atoms gives immediately the ionic formulas $Na^{1+}{}_2Ti^{3+}{}_2Pn^{3-}{}_2O^{2-}$ and $Ba^{2+}Ti^{3+}{}_2Pn^{3-}{}_2O^{2-}$ or, in other form, $Na_2{}^{2+}[Ti_2Pn_2O]^{2-}$ and $Ba^{2+}[Ti_2Pn_2O]^{2-}$. This means identical atomic charge states and identical inter-blocks charge transfer irrespective of the chemical composition and the structural type of ATi_2Pn_2O phases.

To estimate numerically the amount of electrons redistributed between different atoms and between the adjacent blocks $[Ti_2Pn_2O]$ and atomic *A* sheets, we carried out a Bader's analysis and calculated the effective atomic charges (Q^{eff}) listed in Table 6. We see that the actual Q^{eff} differ from the formal ionic charges owing to covalency in blocks $[Ti_2Pn_2O]$; besides, the values of Q^{eff}(Ti) correlate with the lattice parameter *a* (distances d^{Ti-Ti}): as d^{Ti-Ti} increase (for Sb-containing phases as compared with As-containing ones), the values of Q^{eff}(Ti) decrease. Finally, the charge transfer between the adjacent atomic *A* sheets and the blocks $[Ti_2Pn_2O]$ for $Na_2Ti_2As_2O$ (1.61*e*) and $Na_2Ti_2Sb_2O$ (1.58*e*) is higher than for $BaTi_2As_2O$ (1.31*e*) and $BaTi_2Sb_2O$ (1.24*e*).

4. Conclusions

In summary, by means of the first-principles calculations, we studied in detail the main trends in structural, electronic properties

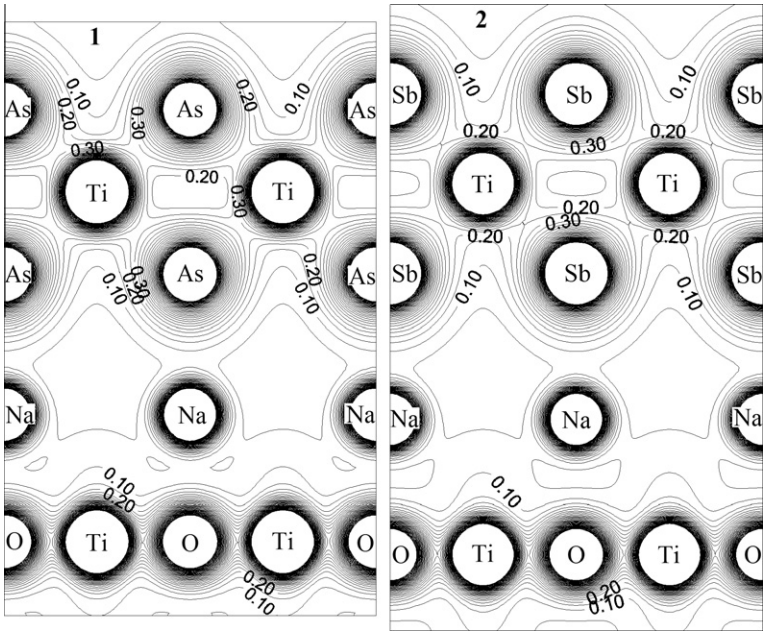

Fig. 6. Charge density maps in (1 1 0) plane for $Na_2Ti_2As_2O$ (1) and $Na_2Ti_2Sb_2O$ (2).

Table 6
Effective atomic charges (Q^{eff}, in e) as calculated within Bader's model for $Na_2Ti_2As_2O$, $Na_2Ti_2Sb_2O$, $BaTi_2As_2O$, and $BaTi_2Sb_2O$.

System	Atom	Q^{eff}	System	Atom	Q^{eff}
$Na_2Ti_2As_2O$	Na	+0.803	$Na_2Ti_2Sb_2O$	Na	+0.792
	Ti	+1.430		Ti	+1.323
	As	−1.545		Sb	−1.431
	O	−1.366		O	−1.362
$BaTi_2As_2O$	Ba	+1.305	$BaTi_2Sb_2O$	Ba	+1.235
	Ti	+1.442		Ti	+1.337
	As	−1.421		Sb	−1.282
	O	−1.337		O	−1.334

and the chemical bonding for the series of quaternary titanium pnictide-oxides: $Na_2Ti_2As_2O$, $Na_2Ti_2Sb_2O$, $BaTi_2As_2O$, and $BaTi_2Sb_2O$, which attracted recently much attention as parent phases for a novel group of layered Fe-free superconducting materials. Our main findings are as follows:

(i) For each pair of isostructural phases ($Na_2Ti_2Pn_2O$ and $BaTi_2Pn_2O$), the isovalent substitutions (As → Sb) lead to *anisotropic deformation* of the crystal structure; this effect is related to strong *anisotropy of inter-atomic bonds*. In turn, in the sequences $Na_2Ti_2As_2O \rightarrow BaTi_2As_2O$ and $Na_2Ti_2Sb_2O \rightarrow BaTi_2Sb_2O$ (i.e. by replacing a double sheet of Na^{1+} ions by a single sheet of Ba^{2+} ions), the main effect is a considerable reduction of the parameter *c*. Simultaneously, a weak reduction of the parameter *a* takes place.

(ii) The near-Fermi electronic bands, which are responsible for the metallic-like behavior of these materials and will be involved in the formation of superconducting state, arise mainly from the Ti 3*d* states of the blocks [Ti_2Pn_2O]. On the contrary, the contributions to the near-Fermi region of the valence states from the double sheets of Na^{1+} or from the single sheet of Ba^{2+} ions are very low or are absent, respectively. Thus, conduction in these materials will be anisotropic and will occur mainly in blocks [Ti_2Pn_2O].

(iii) Our calculations indicate that among the near-Fermi Ti 3*d* states, three orbitals: d_{xy} (which form metal–metal bonds between the neighboring Ti atoms), d_{x2-y2} (directed to O^{2-} ions), and d_{z2} (directed along the *c* axis) give the main contributions to this region and will define the features of the Fermi surfaces. On the contrary, the d_{xz} and d_{yz} orbitals forming the covalent Ti 3*d*–*Pn p* bonds are shifted above and below of the Fermi level.

(iv) The multi-sheet FSs for all the examined phases ATi_2Pn_2O combine the hole-type and electron-type pockets. For $Na_2Ti_2Pn_2O$, their FSs include hole- and electron-type sheets in the form of deformed cylinders (on the lateral sides and in the corners of the BZ, respectively) and electron-like pockets of a complicated convex topology centered at the Γ point. For $BaTi_2Pn_2O$, these electron-like pockets centered at Γ become closed.

(v) Our analysis reveals that for these layered phases the interatomic bonding is of a high-anisotropic character being a mixture of covalent, ionic, and metallic contributions inside blocks [Ti_2Pn_2O], whereas the bonding between blocks [Ti_2Pn_2O] and atomic *A* sheets is of an ionic type. The numerical estimations showed that the actual effective atomic charges differ from the formal ionic charges owing to covalency in blocks [Ti_2Pn_2O], and the amount of electrons redistributed between the adjacent blocks [Ti_2Pn_2O] and atomic *A* sheets differs from that assumed within the simplified ionic model. In particular, the charge transfer to blocks [Ti_2Pn_2O] for $Na_2Ti_2Pn_2O$ is higher than for $BaTi_2Pn_2O$.

Appendix A. Supplementary material

Supplementary data associated with this article can be found, in the online version, at http://dx.doi.org/10.1016/j.jallcom.2013.02.155.

References

[1] Y. Kamihara, T. Watanabe, M. Hirano, H. Hosono, J. Am. Chem. Soc. 130 (2008) 3296.
[2] J. Guo, S. Jin, G. Wang, S. Wang, K. Zhu, T. Zhou, M. He, X. Chen, Phys. Rev. B 82 (2010) 180520R.

[3] R. Pöttgen, D. Johrendt, Z. Naturforsch. B 63 (2008) 1135.
[4] A.L. Ivanovskii, Phys. – Uspekhi 51 (2008) 1229.
[5] Z.A. Ren, Z.X. Zhao, Adv. Mater. 21 (2009) 4584.
[6] J. Paglione, R.L. Greene, Nat. Phys. 6 (2010) 645.
[7] D.C. Johnson, Adv. Phys. 59 (2010) 803.
[8] A.L. Ivanovskii, Physica C 471 (2011) 409.
[9] D. Johrendt, J. Mater. Chem. 21 (2011) 13726.
[10] D. Johrendt, H. Hosono, R.D. Hoffmann, R. Pöttgen, Z. Kristallogr. 226 (2011) 435.
[11] X. Zhu, F. Han, G. Mu, B. Zeng, P. Cheng, B. Shen, H.H. Wen, Phys. Rev. B 79 (2009) 024516.
[12] H. Ogino, Y. Matsumura, Y. Katsura, K. Ushiyama, S. Horii, K. Kishio, J. Shimoyama, Supercond. Sci. Technol. 22 (2009) 075008.
[13] H. Kotegawa, T. Kawazoe, H. Tou, K. Murata, H. Ogino, K. Kishio, J. Shimoyama, J. Phys. Soc. Jpn. 78 (2009) 123707.
[14] X. Zhu, F. Han, G. Mu, P. Cheng, B. Shen, B. Zeng, H.H. Wen, Phys. Rev. B 79 (2009) 220512.
[15] H. Ogino, Y. Katsura, S. Horii, K. Kishio, J. Shimoyama, Supercond. Sci. Technol. 22 (2009) 085001.
[16] M. Tegel, F. Hummel, S. Lackner, I. Schellenberg, R. Pöttgen, D. Johrendt, Ztschr. Anorgan. Allg. Chem. 635 (2009) 2242.
[17] M. Tegel, F. Hummel, Y. Su, T. Chatterji, M. Brunelli, D. Johrendt, EPL 89 (2010) 37006.
[18] I.R. Shein, A.L. Ivanovskii, J. Supercond. Nov. Magn. 22 (2009) 613.
[19] A.L. Ivanovskii, Russ. Chem. Rev. 79 (2010) 1.
[20] H. Ogino, S. Sato, K. Kishio, J. Shimoyama, T. Tohei, Y. Ikuhara, Appl. Phys. Lett. 97 (2010) 072506.
[21] N. Ni, J.M. Allred, B.C. Chan, R.J. Cava, Proc. Natl. Acad. Sci. USA 8 (2011) E1019.
[22] C. Löhnert, T. Stürzer, M. Tegel, R. Frankovsky, G. Friederichs, D. Johrendt, Angew. Chem. Int. Ed. 50 (2011) 9195.
[23] R. Nath, V.A. Garlea, A.I. Goldman, D.C. Johnston, Phys. Rev. B 81 (2010) 224513.
[24] G. Wang, M. Zhang, L. Zheng, Z. Yang, Phys. Lett. A 374 (2010) 4727.
[25] I.R. Shein, V.V. Bannikov, A.L. Ivanovskii, Phys. Status Solidi B 248 (2011) 2165.
[26] T. Yajima, K. Nakano, F. Takeiri, T. Ono, Y. Hosokoshi, Y. Matsushita, J. Hester, Y. Kobayashi, H. Kageyama, J. Phys. Soc. Jpn. 81 (2012) 103706.
[27] P. Doan, M. Gooch, Z. Tang, B. Lorenz, A. Möller, J. Tapp, P.C.W. Chu, A.M. Guloy, J. Am. Chem. Soc. 134 (2012) 16520.
[28] E.A. Axtell, T. Ozawa, S.M. Kauzlarich, R.R.P. Singh, J. Solid State Chem. 134 (1997) 423.
[29] F.F. de Biani, P. Alemany, E. Canadell, Inorg. Chem. 37 (1998) 5807.
[30] T.C. Ozawa, R. Pantoja, E.A. Axtell, S.M. Kauzlarich, J.E. Greedan, M. Bieringer, J.W. Richardson, J. Solid State Chem. 153 (2000) 275.
[31] T.C. Ozawa, S.M. Kauzlarich, M. Bieringer, J.E. Greedan, Chem. Mater. 13 (2001) 1804.
[32] T.C. Ozawa, S.M. Kauzlarich, J. Cryst. Growth 265 (2004) 571.
[33] R.H. Liu, D. Tan, Y.A. Song, Q.J. Li, Y.J. Yan, J.J. Ying, Y.L. Xie, X.F. Wang, X.H. Chen, Phys. Rev. B 80 (2009) 144516.
[34] H.F. Wang, Y.J. Yan, J.J. Ying, Q.J. Li, M. Zhang, N. Xu, X.H. Chen, J. Phys.: Condens. Matter. 22 (2010) 075702.
[35] T. Yajima, K. Nakano, F. Takeiri, J. Hester, T. Yamamoto, Y. Kobayashi, N. Tsuji, Y. Kim, A. Fujiwara, H. Kageyama, J. Phys. Soc. Jpn. 82 (2013) 013703.
[36] Y. Huang, H.P. Wang, W.D. Wang, Y.G. Shi, N.L. Wang, arXiv: 1301.1216 (2013).
[37] W.E. Pickett, Phys. Rev. B 58 (1998) 4335.
[38] X.W. Yan, Z.Y. Lu, arXiv:1210.3481 (2012).
[39] D.J. Singh, arXiv:1209.4668 (2012).
[40] A. Subedi, arXiv:1210.0499 (2012).
[41] P. Blaha, K. Schwarz, G.K.H. Madsen, D. Kvasnicka, J. Luitz, WIEN2k, An Augmented Plane Wave Plus Local Orbitals Program for Calculating Crystal Properties, Vienna University of Technology, Vienna, 2001.
[42] J.P. Perdew, K. Burke, M. Ernzerhof, Phys. Rev. Lett. 77 (1996) 3865.
[43] P.E. Blöchl, O. Jepsen, O.K. Anderson, Phys. Rev. B 49 (1994) 16223.
[44] R.F.W. Bader, Atoms in Molecules: A Quantum Theory, International Series of Monographs on Chemistry, Clarendon Press, Oxford, 1990.
[45] A. Adam, H.U. Schuster, Z. Anorg, Allg. Chem. 584 (1990) 150.
[46] E. Clementi, D.L. Raimond, W.P. Reinhardt, J. Chem. Phys. 47 (1967) 1300.
[47] Ch. Walti, E. Felder, C. Degen, G. Wigger, R. Monnier, B. Delley, H.R. Ott, Phys. Rev. B 64 (2001) 172515.